# Elasticity of weakly aggregating polystyrene latex dispersions

R. de Rooij, D. van den Ende, M. H. G. Duits, and J. Mellema
*Rheology Group, Department of Applied Physics, University of Twente, P.O. Box 217, 7500 AE Enschede, The Netherlands*
(Received 7 September 1993)

The elastic behavior of a weakly aggregating polystyrene latex dispersion was investigated using a homemade controlled stress rheometer and commercially available dynamic rheometers. Both the creep measurements and the oscillatory experiments show the absence of a yield stress. The low-shear-limiting viscosity obtained with the controlled stress apparatus shows a power-law dependence upon volume fraction with a power of $5.3\pm0.3$. Combining the data of the different rheometers, the storage shear modulus $G'$ at high frequencies was found to depend upon volume fraction with a power of $4.6\pm0.3$, being in line with earlier data mentioned in the literature. Using an additional exponent, i.e., one describing the critical strain above which the material deforms nonlinearly, the fractal dimension $d_f$ and the upper and lower bounds of the structural parameter $\varepsilon$ were obtained. The latter is a measure for the degree of anisotropy of the network skeleton. The values $d_f=2.0\pm0.2$ and $0.5\leq\varepsilon\leq1$ are consistent with a model based on noncentral or bond-bending interactions. It was shown that the structural parameters and hence the microstructure change significantly when going from rest to high shear rates. Thus, in general, one cannot use the results obtained with one type of experiment in another type of experiment.

PACS number(s): 82.70.Dd, 62.20.Hg

## I. INTRODUCTION

The question of whether aggregating dispersions have a finite low-shear-limiting viscosity or a yield stress and also a nonzero equilibrium shear modulus (which is the modulus measured at infinitesimally small deformations) has been a matter of controversy for quite some time. Solidlike behavior has been reported by Sonntag and Russel [1] and Chen and Russel [2]. These authors measured the complex modulus in oscillatory shear and found a low-frequency plateau in the storage modulus. One can argue that this is no proof for the existence of a finite zero-frequency limit of the storage modulus, since one can always raise the question of what would happen if one were able to measure at still lower frequencies. Furthermore, Chen and Russel in the same study [2] showed the result of a creep measurement on an aggregating silica dispersion at a shear stress far below the reported yield stress, which was contradictory to the idea of a rest modulus because the strain increased linearly with time after imposition of a constant stress, while the deformation did not completely recover after cessation of the applied stress. However, this could perhaps be ascribed to the fact that the only reported creep experiment was performed on a sample just below its melting point or percolation threshold, which might still exhibit fluidlike behavior. No creep experiments were reported above the percolation threshold, so it remains unclear if the observed creep behavior is characteristic for the entire range of experimental conditions covered by the dynamic measurements.

Buscall, McGowan, and Morton-Jones [3] measured the high-frequency limit of the storage modulus and the steady shear viscosity as a function of shear rate for a number of volume fractions. A Newtonian low-shear-rate plateau was found, indicating the absence of a yield stress. Russel [3] argued however, that the detected plateau could be due to wall slip, which may be difficult to avoid at high relative viscosities $\geq10^3$. Recently, Buscall, McGowan, and Morton-Jones [4] reconsidered their earlier experiments and performed new measurements using roughened cylinders. They concluded that the earlier results were indeed influenced by wall slip. However, in the more recent experiments they again found a low-shear-rate plateau in the viscosity.

Patel and Russel [5] reported reproducible yield stresses in aggregating polystyrene latex–dextran dispersions. They did not show any plots of the strain as a function of time; hence, it is not clear whether the angular displacement could be measured with sufficient accuracy with the apparatus used.

At low volume fractions the network formed by an aggregating dispersion has been shown to have a fractal structure [6], i.e., the number of particles inside a sphere depends upon the radius of the latter via a power law, the exponent of which is called the fractal dimension. The values of the fractal dimension under different conditions are well established now. As a result of the fractal nature of the microstructure, the high-frequency storage modulus (and other quantities depending on the microstructure) of aggregating dispersions as a function of volume fraction also shows a power-law scaling behavior, i.e., $G'\propto\phi^{\gamma_1}$, with $\gamma_1$ depending on the age of the sample [1]. The values most often mentioned [2,7–9] lie in the range from 3.7–4.5, $\gamma_1$ being higher for older samples. Low values of $\gamma_1$ were shown to be indicative of anisotropic structures or low fractal dimensions, whereas higher values indicate more isotropic structures or higher fractal dimensions [10,11].

From a theoretical point of view, a number of authors pointed out that for spheres, central interactions alone cannot be responsible for static elastic behavior at small

 

deformations [11,12] because the particles would be able to rotate freely around each other. Since the usual electrostatic, van der Waals, and steric forces from colloid chemistry are central, it is difficult to understand elastic behavior of aggregating dispersions in terms of these pair-interaction potentials. These difficulties could be avoided if one assumes particle chains in the network to be straight. In some cases, such as, e.g., aggregation in shear flow [13], this assumption is perhaps not unreasonable, but if aggregation takes place in the absence of shear flow, it is difficult to see why one would expect straight chains, especially at higher-volume fractions. Then we have to imagine possible causes of noncentral interactions as an origin of elasticity. In our model dispersion a surfactant layer is adsorbed onto the surface of the spherical particles. For particles with polymer layers adsorbed on their surfaces, a number of authors recently showed [14–18] that for two interpenetrating layers, there is a force parallel to the particle surfaces, resisting shear and hence hindering rotation of particles around each other. Though it is difficult to quantify the magnitude of this force for our model system with adsorbed surfactant instead of polymer, qualitatively it seems plausible that a slight interpenetration of surfactant layers may indeed be the cause of some bond-bending component of the interparticle force on time scales shorter than the relaxation time of "entanglements" between surfactants belonging to different layers, thus leading to a shear modulus at higher frequencies. Another possible cause of bond-bending interactions may be inhomogeneous adsorption of surfactant on the particle surface. In this case it will be energetically favorable for two particles to make contact in the area of relatively low surfactant density. Moreover, if one has a surfactant layer which is not *grafted* but is *adsorbed* onto the surface, the adsorption equilibrium may change locally when two particles meet. Due to the driving force caused by the van der Waals attraction, surfactant may desorb in the area of contact, which results in a locally higher attractive energy and also a bond-bending force. Finally, though viewed with an electron microscope the particles seem to be spherical, it is not clear whether they are spherical on smaller length scales. Any deviation from the spherical shape would also cause a locally higher attractive energy. The last three cases may also lead to the existence of a *static* shear modulus at small deformations.

In the present paper rheological experiments are reported on a "weakly" aggregating polystyrene latex dispersion, i.e., the attractive interaction energy between two particles ranges roughly between $4k_BT$ and $10k_BT$. To this end, a surfactant with a suitable chain length is adsorbed onto the particle surfaces [19]. At saturation adsorption a dense layer is present, causing steric repulsion. Hence, after addition of electrolyte, the system will aggregate only weakly, since the dense layer effectively decreases the strength of the attraction. The advantage of a weakly aggregating model system is that at these relatively low attractive energies, particle bonds are rather easily broken under shear, while at the same time the attraction is strong enough to prevent fast thermal breakup of bonds in the absence of shear, thus facilitating experiments on reproducible structures.

Two kinds of experiments were performed. First, a controlled stress rheometer developed in our own laboratory [20] was used to perform creep measurements for a number of volume fractions between 0.02 and 0.30. The apparatus is capable of applying very small stresses (down to 0.6 mPa) and of measuring very small angular displacements (down to $10^{-6}$ rad). Since the applied stresses were well below the yield stresses reported in the literature [5], it was expected that in the case of a yield stress, the angular displacement as a function of time should reach a constant value at each shear stress. Moreover, application of a range of stresses enabled a check on the linearity of stress-strain experiments. In the absence of a yield stress, a low-shear-limiting viscosity was expected.

Second, dynamic moduli were measured in the frequency range between 0.001 and 5 Hz in order to investigate whether or not a low-frequency plateau in the storage modulus could be detected and to see if the results of the two independent experiments could be related to each other. It was hoped that through the use of the accurate equipment, some new light could be shed on the question of whether or not at least the specific model system used possesses a yield stress under certain conditions. Furthermore, we intended to correlate experimental data with a certain model for the microstructure. Thus a number of parameters describing the microstructure of the aggregating model dispersion were determined. It is noted that the model assumes a fractal network to be formed over the entire range of volume fractions mentioned above, though this may be questionable at the higher volume fractions ($\phi > 0.15$). However, it will be shown that the measured rheological quantities corroborate the same scaling behavior for all the volume fractions considered.

## II. THEORETICAL

### A. Relation between retardation and relaxation

In the controlled stress experiments a stress $\sigma(t)=\sigma_0 H(t)$, with $H(t)$ the Heaviside unit step function, is applied, after which the strain $\gamma(t)$ is measured. From the theory of linear viscoelasticity [21], one can derive a general form of the retardation function $J(t)\equiv[\gamma(t)]/\sigma_0$, i.e.,

$$J(t)=H(t)\left[J_g+\frac{t}{\eta(0)}+\sum_k J_k(1-e^{-t/t_k})\right], \qquad (2.1)$$

where $J_g$ is the glass compliance, $\eta(0)$ the low shear limit of the steady shear viscosity, and $J_k$ the retardation strength at retardation time $t_k$. We note that (2.1) may only be used in the *linear* case, i.e., when $J(t)$ does not depend upon $\sigma_0$.

Considering the inverse experiment, one can also derive the general form of the stress $\sigma(t)$ as a function of time after imposing a stepwise strain $\gamma(t)=\gamma_0 H(t)$. The function $G(t)\equiv[\sigma(t)]/\gamma_0$ has the form [21]

$$G(t)=\eta'(\infty)\delta(t)+H(t)\left[G_0+\sum_k G_k e^{-t/\tau_k}\right], \quad (2.2)$$

where $\eta'(\infty)$ is the real part of the complex viscosity at infinite frequency, $G_0$ the equilibrium modulus, and $G_k$ the relaxation strength at relaxation time $\tau_k$. Defining $J^*(\omega)\equiv J'-iJ''$ and $G^*\equiv G'+iG''$ as the Fourier transforms of $dJ(t)/dt$ and $dG(t)/dt$, respectively, the relation between these is given by [21]

$$J^*G^*=1 \quad (2.3)$$

or

$$J'G'=-J''G''+1 , \quad (2.4a)$$

$$J'G''=J''G' . \quad (2.4b)$$

Performing the Fourier transforms gives

$$J'(\omega)=J_g+\sum_k J_k\left[1-\frac{\omega^2}{\omega^2+1/t_k^2}\right],$$
$$J''(\omega)=\frac{1}{\eta(0)\omega}+\sum_k J_k\frac{\omega/t_k}{\omega^2+1/t_k^2} \quad (2.5)$$

and

$$G'(\omega)=G_0+\sum_k G_k\frac{\omega^2}{\omega^2+1/\tau_k^2}\equiv\omega\eta'' ,$$
$$G''(\omega)=\eta'(\infty)\omega+\sum_k G_k\frac{\omega/\tau_k}{\omega^2+1/\tau_k^2}\equiv\omega\eta' . \quad (2.6)$$

Note that the existence of an equilibrium modulus $G_0$ implies a low-frequency plateau in $G'(\omega)$. Substituting (2.5) and (2.6) into (2.4), one obtains two relations that must be satisfied for all $\omega$. These relations are generally valid within the formalism of linear viscoelasticity. Next, we consider the limits for $\omega\to 0$ and $\omega\to\infty$ of (2.4a) and (2.4b), in order to distinguish some special classes of materials. Taking $\omega\to 0$ in (2.4a) yields

$$G_0\left[J_g+\sum_k J_k\right]=-\frac{\eta'(0)}{\eta(0)}+1 . \quad (2.7)$$

Considering (2.4a) for $\omega\to\infty$ gives

$$J_g\left[G_0+\sum_k G_k\right]=-\frac{\eta'(\infty)}{\eta(0)}-\sum_k\eta'(\infty)J_k/t_k+1 . \quad (2.8)$$

Doing the same for (2.4b), one finds

$$\lim_{\omega\to 0}\frac{G_0}{\eta(0)\omega}=0 \quad (2.9)$$

and

$$\lim_{\omega\to\infty}J_g\eta'(\infty)\omega=0 , \quad (2.10)$$

respectively.

One now can distinguish between four classes of materials which satisfy Eqs. (2.7)–(2.10), i.e.,

(1) $J_g>0$, $\eta'(\infty)=0$; $G_0>0$, $\eta(0)=\infty$. For both short and long times such a material is *elastic.*

(2) $J_g>0$, $\eta'(\infty)=0$; $G_0=0$, $\eta(0)>0$. Materials in this class behave *elastically* at *fast* deformations and *viscous* at *slow* deformations.

(3) $J_g=0$, $\eta'(\infty)>0$; $G_0>0$, $\eta(0)=\infty$. In this case the material behaves *viscous* at *fast* deformations and *elastically* at *slow* deformations.

(4) $J_g=0$, $\eta'(\infty)>0$; $G_0=0$, $\eta(0)>0$. Materials belonging to this class behave *viscous* on both short and long time scales.

Thus one can conclude that if in a *linear* measurement $J(t)$ does not reach a constant value, i.e., $\eta(0)>0$, $G_0$ must be zero and the material under investigation has no yield stress. Considering for the time being a class-1 or -2 material, one finds from (2.8)

$$J_g=\frac{1}{G_0+\sum_k G_k}=\frac{1}{G'(\infty)} , \quad (2.11)$$

where in the first equation $G_0=0$ for a class-2 material. Using (2.11), creep experiments can be related to dynamic measurements, provided one finds a finite $J_g$. We will show in Sec. IV that the latter is indeed the case.

### B. Mean relaxation time from creep experiments

One may wish to extract a characteristic *relaxation* time from creep experiments, which can be compared to a time obtained with dynamic measurements. To this end, we first write the complex viscosity $\eta^*(\omega)$ as [21]

$$\eta^*(\omega)=\int_{-\infty}^{\infty}e^{-i\omega t}G(t)dt , \quad (2.12)$$

i.e., as the Fourier transform of the relaxation function $G(t)$ given by (2.2). A mean relaxation time $\tau_M$ or characteristic time scale of change of the memory function $G(t)$ can be defined by

$$\tau_M=\frac{\int_{-\infty}^{\infty}tG(t)dt}{\int_{-\infty}^{\infty}G(t)dt}=\begin{cases}\infty , & G_0>0 \quad (2.13a)\\ \sum_k G_k\tau_k^2\Big/\left[\sum_k G_k\tau_k+\eta'(\infty)\right]=\sum_k G_k\tau_k^2/\eta'(0) , & G_0=0 . \quad (2.13b)\end{cases}$$

Writing $G_k\tau_k=\eta_k$, one sees that $\tau_m$ is the weighted average of the relaxation times $\tau_k$ with $\eta_k$ as a weighting function. Restricting ourselves now to the case $G_0=0$, i.e., a class-2 or -4 material, we have $\eta'(0)=\eta(0)$ in (2.13b). On the other hand, one has in the frequency domain the relation

$$J'(\omega)=\frac{G'(\omega)}{G'(\omega)^2+G''(\omega)^2} . \tag{2.14}$$

Defining the steady-state compliance $J_e$ by $J_e\equiv J'(0)$, one finds, after taking the limit for $\omega\rightarrow 0$ of (2.14) and using (2.6) and (2.13b),

$$\tau_M=J_e\eta(0) , \tag{2.15}$$

which allows evaluation of the mean relaxation time from creep experiments, in which $J(t)$ is measured. Hence, for a class-2 or -4 material this characteristic time may then be compared to the time scale obtained by dynamic measurements.

### C. Scaling behavior of rheological quantities

Several authors [8,10,22] have modeled power-law behavior of the elastic modulus for fractal structures, which arise at low volume fractions of primary particles, i.e., $\phi<0.1$. All these approaches assume bond-bending interactions between the primary particles which form skeleton chains combined into a space-filling network. Although in the Introduction we pointed out that it is not straightforward to imagine bond-bending forces, it is possible, and we will follow the same approach as other authors [8,10,22] to see if in this way a plausible interpretation of the measurements can be found.

Kantor and Webman [23] showed that in the case of both central and noncentral interactions, the latter dominate for long particle chains. They found for the elastic force constant $k_e$ of a particle chain with noncentral interactions

$$k_e\propto\frac{1}{N_{\rm ch}R_\perp^2} , \tag{2.16}$$

where $R_\perp$ is the radius of gyration of the chain projected on the plane perpendicular to the line connecting the ends of the chain and $N_{\rm ch}$ the number of particles in the chain.

In the following we only consider the skeleton chains of the network, by which any external forces are transmitted. Brown [10] and Shih *et al.* [8] assumed the chains to be isotropic, i.e., $R_\perp\approx\xi$, where $\xi$ is the correlation length of the space-filling network. The latter may be viewed as consisting of a number of connected *blobs* with radius $\xi$ [24]. Each blob is assumed to have one skeleton chain with length $\xi$. However, a more general description may be obtained by taking into account the anisotropy of the chain [22], i.e.,

$$R_\perp\propto\xi^\varepsilon , \tag{2.17}$$

with $0\le\varepsilon\le 1$. The case $\varepsilon=0$ applies to a straight chain, while $\varepsilon=1$ applies to a purely isotropic chain. Furthermore, the number of particles $N_{\rm ch}$ in the chain is related to the correlation length $\xi$ by [24]

$$N_{\rm ch}\propto\xi^{d_{\rm ch}} . \tag{2.18}$$

The exponent $d_{\rm ch}$ is called the chemical dimension and must be at least 1 to provide a closed path. The upper bound of $d_{\rm ch}$ is given by $\min(d_f,\frac{5}{3})$, the value $\frac{5}{3}$ pertaining to a self-avoiding chain. Computer simulations have suggested that $d_{\rm ch}=1.35$ for a three-dimensional (3D) percolation network [25]. It is noted that the exponents $\varepsilon$ and $d_{\rm ch}$ are coupled in some way, e.g., for straight chains one has $\varepsilon=0$ and $d_{\rm ch}=1$.

Now the shear modulus $G_0$ is given by the $\xi$ dependence:

$$G_0\propto k_e/\xi\propto\xi^{-1-2\varepsilon-d_{\rm ch}} . \tag{2.19}$$

If one is dealing with a fractal structure, i.e., [24]

$$\xi\propto\varphi^{1/(d_f-3)} , \tag{2.20}$$

where $\phi$ is the volume fraction of primary particles, one finally obtains

$$G_0\propto\phi^{(1+2\varepsilon+d_{\rm ch})/(3-d_f)}\equiv\phi^{\gamma_1} . \tag{2.21}$$

We note that in the following (as have other investigators [8–10]), the storage modulus $G'(\infty)$ at infinite frequency is assumed to have the *same* power-law behavior as $G_0$. More sophisticated modeling would involve much more complicated calculations than the scaling considerations given in this work.

Now we derive a simple expression for the yield stress $\sigma_y$ of a fractal network. Writing down the critical energy per skeleton chain, thus assuming only one chain is loaded, one has

$$UN_{\rm ch}=f_{\rm ext}\Delta\xi , \tag{2.22}$$

where $U$ is the bending energy needed to break one bond between two primary particles, $f_{\rm ext}$ is an external force, and $\Delta\xi$ is the deformation of a blob. Using $f_{\rm ext}=k_e\Delta\xi$ and (2.16), (2.17), and (2.22), one finds

$$f_{\rm ext}=(k_eUN_{\rm ch})^{1/2}\propto\xi^{-\varepsilon} , \tag{2.23}$$

which yields

$$\sigma_y\approx\frac{f_{\rm ext}}{\xi^2}\propto\xi^{-2-\varepsilon}\propto\phi^{(2+\varepsilon)/(3-d_f)}\equiv\phi^{\gamma_2} . \tag{2.24}$$

For isotropic chains (i.e., $\varepsilon=1$), Wessel and Ball [26] derived a similar expression for $\sigma_y$ in a different way. One sees that $\gamma_1\ge\gamma_2$.

The experiments described in this paper all deal with *linear* viscoelastic behavior. Above a certain critical strain, however, this is no longer the case. Shih *et al.* [8] give an expression for the limit of linearity $\gamma_{\rm crit}$ assuming isotropic chains. They start by writing the microscopic deformation $\Delta\xi$ in terms of the macroscopic deformation $\Delta L$, i.e.,

$$\Delta\xi\approx\frac{\Delta L}{L/\xi} . \tag{2.25}$$

Generalizing their approach, we next write the force $f_{ext}$ on a blob as

$$f_{ext} = k_e \Delta\xi \propto \frac{1}{\xi^{2\varepsilon + d_{ch}}} \frac{\Delta L}{L/\xi} , \quad (2.26)$$

where (2.16) has been used, and we again take into account the anisotropy of the chains. A bond breaks if the force $f_{ext}$ on it exceeds a critical value, which may be set to unity since we are only interested in scaling behavior. Hence, $\gamma_{crit}$ is given by

$$\gamma_{crit} = \frac{\Delta L}{L} \propto \xi^{2\varepsilon - 1 + d_{ch}} \propto \phi^{(1 - 2\varepsilon - d_{ch})/(3 - d_f)} \equiv \phi^{\gamma_3} . \quad (2.27)$$

Shih *et al.* measured $\gamma_3$ for two kinds of boehmite alumina gels and found $\gamma_3 = -2.1$ and $\gamma_3 = -2.3$. The exponents $\gamma_1$, $\gamma_2$, and $\gamma_3$ contain three unknowns, i.e., the structural parameters $d_f$, $d_{ch}$, and $\varepsilon$. Thus, from separate determinations of these exponents, one can in principle obtain values of the structural parameters. In this work measurements of $\gamma_1$ and $\gamma_3$ will be reported.

## III. EXPERIMENT

### A. The model system

The system we investigated was described earlier by Goodwin *et al.* [19] and consists of a polystyrene latex dispersion with a negative surface charge and a nonionic surfactant, i.e., $C_{12}E_6$, adsorbed onto the surface of the particles. At saturation adsorption a dense layer is present, causing steric repulsion at short distances and thereby reducing the depth of the (van der Waals) potential well. Goodwin *et al.* [19] supposed that the surfactant molecules are fully stretched and estimated the layer thickness to be 3.85 nm. After addition of a suitable amount of electrolyte, the particles will aggregate due to screening of the electrostatic repulsion. Since due to the chain length of the particular surfactant chosen the potential well is rather shallow (less than $10k_BT$), this aggregation is reversible, i.e., the structure can be broken down again by shearing the sample at a high shear rate.

### B. Materials

Two monodisperse polystyrene latices (hereafter referred to as *latex A* and *latex B)* were prepared without emulsifier using the method described by Goodwin *et al.* [27]. It should be noted, however, that in the case of latex *A*, we made some modifications. Instead of a three-necked flask, we used a 500-ml borosilicate bottle. After addition of 425 ml water and 50 ml styrene nitrogen was purged through. Hereafter, the bottle was sealed and placed in a thermostat bath at 70 °C. In this bath the bottle was rotated end over (at 40 rpm) to ensure thorough mixing. After 1 h, the bottle was shortly removed in order to add 0.25 g $K_2S_2O_8$ dissolved in 25 ml water, and placed back again. The advantages of this method are that the reaction takes place in a closed system and that the styrene is better mixed with the water. In the case of latex *B*, the preparation as described by Goodwin *et al.* was followed, except that now a 2-liter three-necked flask was used in order to obtain a larger yield. The quantities added were 1700 ml water, 200 ml styrene, and 1.49 g $K_2S_2O_8$ (dissolved in 100 ml water). As with latex *A*, the reaction took place at 70 °C.

The latices were purified with an Amicon TFC10 ultrafiltration apparatus. The number averaged particle radii as determined with electron microscopy were 200 and 250 nm for latex *A* and latex *B*, respectively. Conductometric titration revealed no weak acid groups on the surface of the particles, while the surface charge densities due to $SO_4^-$ groups were 5.8 and 5.1 $\mu C/cm^2$ for latices *A* and *B*, respectively.

After purification, $C_{12}E_6$ (Nikko Chemicals Co.) was added. The samples were rotated end over for 24 h in order to attain equilibrium adsorption. The amount of $C_{12}E_6$ was such that an equilibrium concentration of $2 \times 10^{-4}$ mol/l was reached [19]. Finally, NaCl was added, resulting in a concentration of 0.7 mol/l. This concentration was high enough to cause aggregation, as could be seen with a light microscope. A slight movement of the slide caused disaggregation to occur, confirming that the sample was only weakly aggregated.

Samples of latex *A*, with volume fractions of 0.027, 0.036, 0.043, 0.074, 0.104, and 0.151 (±5%) were prepared from a stock dispersion by addition of a $C_{12}E_6$-NaCl solution to the concentrations indicated above. Similarly, samples of latex *B* with volume fractions of 0.118, 0.172, 0.230, and 0.287 (±3%) were prepared.

### C. Rheological measurements

#### 1. *Creep experiments*

For the creep experiments we used a controlled stress rheometer with a double-gap geometry, capable of applying small shear stresses (down to $\approx 0.6$ mPa) and detecting small angular displacements (down to $\approx 10^{-16}$ rad). This instrument has been developed in our laboratory [20]. For a number of volume fractions ranging from 0.02 to 0.30, shear stresses between 6 mPa and 1 Pa were applied in the following way: the samples of latex *A* were presheared for a few minutes at a high motor speed. The cylinder speeds, however, were low due to the high viscosities involved. The samples of latex *B* were not presheared, because the viscosities were too high to move the measuring cylinder at an appreciable speed. After a waiting period of 1 to 4 h to allow for formation of a network, a small stress was applied for a certain period (usually between 30 and 200 s, depending on the volume fraction). During this period the angular displacement as a function of time was recorded every 0.5 s, and after cessation of the applied stress, the elastic recoil to a new equilibrium position was measured in the same way during more than 200 s. Hereafter, a higher stress was applied and this procedure was repeated for about 50 stresses per volume fraction.

#### 2. *Dynamic experiments*

The dynamic experiments were performed with two rheometers, i.e., a Bohlin VOR, suitable for measuring

moduli $G' \geq 1$ Pa and a Rank Pulse Shearometer, which was designed especially for highly elastic materials (50 Pa $< G' <$ 500 kPa). At volume fractions $\phi \geq 0.074$, the storage and loss moduli were measured in the frequency range between $10^{-2}$ and 5 Hz using the Bohlin apparatus. At volume fractions lower than 0.074, the moduli were too low to be measured. By varying the applied maximum strain, a check on the limits of linearity was performed. With the Pulse Shearometer only one frequency can be applied (250 Hz). Since this rheometer only works well at storage moduli larger than 50 Pa, it was used for higher volume fractions (latex *B*).

Since the moduli increase on very long time scales, all the Bohlin measurements were done after a waiting period of 13 000 s. With the Pulse Shearometer a waiting period of more than 12 h was taken prior to the measurements. To avoid evaporization of the sample, a solvent trap was used on the Bohlin. For the Pulse Shearometer this was not necessary since the sample was already isolated from the outer atmosphere.

With the Bohlin the effect of preshearing of the sample on the dynamic moduli was investigated in the following way: After a waiting period of 13 000 s, the moduli as a function of frequency without preshearing were measured. Then a low shear rate of about 0.1 $s^{-1}$ was applied for 32 min. After another waiting period of 13 000 s, a new frequency sweep was done. Finally, the same procedure was repeated with a shear rate of about 100 $s^{-1}$. Thus, we were able to examine the effect of shear history of the sample on the magnitude of the moduli as a function of frequency. Both the creep and the dynamic experiments were done at room temperature (298.15 K).

## IV. RESULTS

### A. Creep experiments

At each volume fraction the experimental data, i.e., the angular displacement as a function of time for a number of shear stresses, were treated in the following way: First, by plotting the jump in the displacement after applying the stress as a function of the latter, a check on the linearity of the measurements was performed. At each volume fraction, the relation between jump and stress turned out to be linear (in some cases up to a certain critical stress). The displacement-time curves for stresses $\sigma_0$ in the linear regime were then averaged by dividing each point by the appropriate stress, adding the curves and dividing by the number $n$ of curves. This resulted in a "master curve"

$$M(t) \equiv \langle \theta(t)/\sigma_0 \rangle \equiv \frac{1}{n} \sum \frac{\theta_i(t)}{\sigma_{0,i}}$$

at each volume fraction. Here, $\theta_i(t)$ is the angular displacement at time $t$, relative to the *original* zero position (i.e., before the first stress was applied). The averaged retardation function $\langle J(t) \rangle$ can be obtained from $M(t)$ in the following way: By definition, $\langle J(t) \rangle \equiv \langle \gamma(t)/\sigma_0 \rangle$, where $\gamma(t)$ is the strain at time $t$. From the geometry of the rheometer, one can estimate

$$\gamma(t) \cong 10.8[\theta(t) - \theta(0)].$$

Hence,

$$\langle J(t) \rangle = 10.8 M(t) - C ,$$

where $C \equiv 10.8 \langle \theta(0)/\sigma_0 \rangle$ is an offset due to the fact that all the displacements are taken relative to the original zero position. In Figs. 1 and 2 typical results are shown.

The steady-state compliance, glass compliance, and viscosity are determined from the curves in the way indicated in Fig. 1 (see also Sec. II A). Apparently, the measurements indicate that we are dealing with a class-2 material, so (2.11) and (2.15) can be used. The instantaneous jump after imposing the stress is determined by a polynomial fit. For latex *A* the viscosity determined from the recovery is about three times higher than the viscosity determined from the slope of the curve as indicated in Fig. 1, being an indication that the time $t_0$ of application of the stress was chosen too short for all the retardation processes to have taken place. Therefore, the viscosities were determined from the recovery. It should be noticed, however, that since the recovery was not yet completed after the time scale of the experiments (i.e., the slope of the curve after cessation of the stress was still slightly negative before application of the next stress), the viscosities determined in this way are lower bounds of the real viscosities.

In the case of latex *B* both ways of obtaining the viscosity gave the same results and thus for this latex the times chosen were long enough. At the highest volume fraction the cylinder returned *below* its original position after cessation of the stress. This turned out to be caused by drift of the autocollimator signal. Separate measurements of this effect on the time scale of the creep experiments (i.e., 4 h) yielded a drift of $-(1.0 \pm 0.5) \times 10^{-9}$ rad/s, which was used to correct the data at $\phi = 0.287$. In Fig. 2 the corrected $M(t)$ is shown. At all other volume fractions the correction was negligible. The data plotted in Fig. 2 are the worst as far as noise is con-

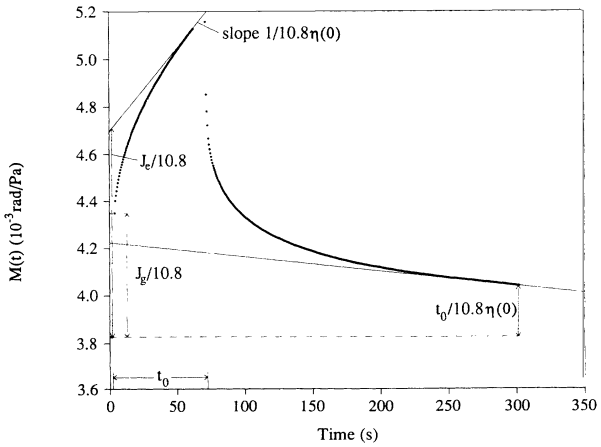


FIG. 1. Typical example of a master curve $M(t)$ measured with the controlled stress rheometer at low volume fractions. The master curve was obtained for latex *A* at $\phi = 0.104$. For averaging, 8 curves were used.

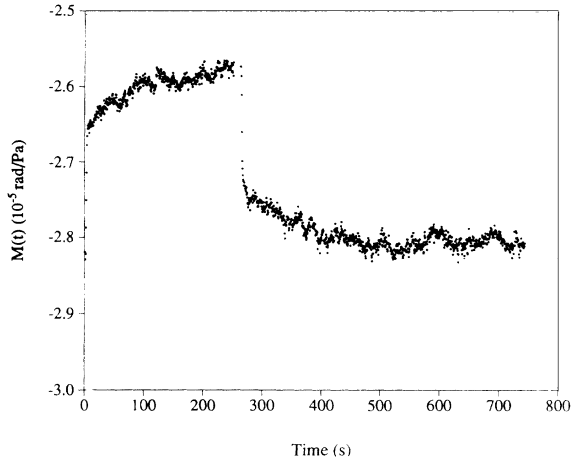


FIG. 2. Typical example of a master curve $M(t)$ measured with the controlled stress rheometer at high volume fractions. The master curve was obtained for latex $B$ at $\phi=0.287$. For averaging, 15 curves were used, considerably reducing noise.

cerned, i.e., in this case the strains are so small that the bounds of the apparatus specifications are reached. All other results looked rather like the graph shown in Fig. 1.

The values of $J_g$ as a function of $\phi$ were converted to $G'(\infty)$ using (2.11). A discussion of the results is given in Sec. IV C.

### B. Dynamic experiments

The results of the dynamic measurements are shown in Figs. 3 and 4 for latices $A$ and $B$, respectively. The data of both dynamic rheometers are shown, while the $G'(\infty)$ extracted from the creep experiments are also plotted for comparison. The applied strains were smaller than $10^{-3}$ in all experiments, this being the lowest limit of linearity $\gamma_{crit}$ determined from measurements at 1 Hz.

The values of $G'$ measured with the Pulse Shearometer (latex $B$) appear to agree reasonably well with the low-

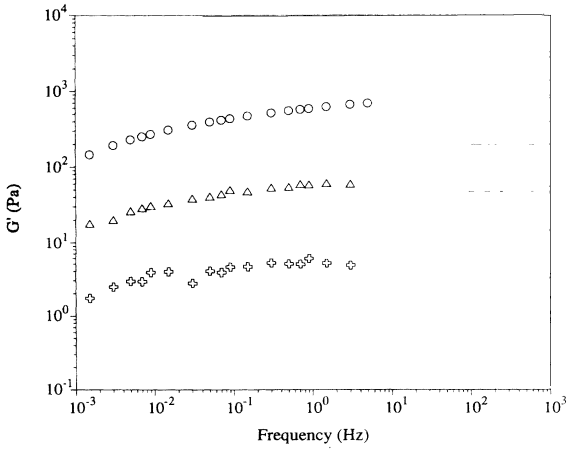


FIG. 3. Storage modulus as a function of frequency for latex $A$ at volume fractions $\phi=0.074$ (◇), 0.104 (△), and 0.151 (○). Also indicated are $G'(\infty)$ obtained from creep experiments at $\phi=0.074$ (dashed line) and $\phi=0.104$ (dot-dashed line).

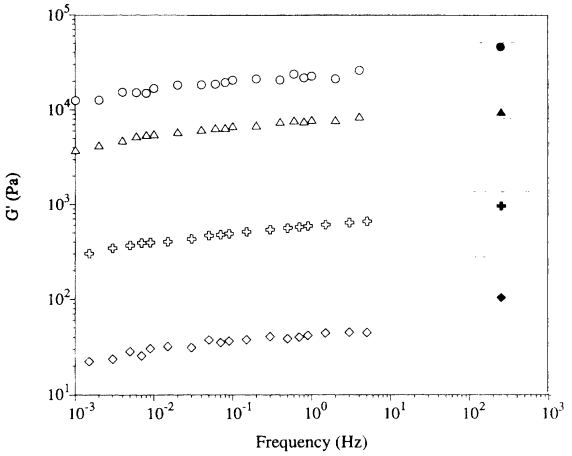


FIG. 4. Storage modulus as a function of frequency for latex $B$ at volume fractions $\phi=0.118$ (◇), 0.172 (◇), 0.230 (△), and 0.287 (○). Also indicated are $G'(\infty)$ obtained from creep experiments (lines in increasing order of volume fraction) and $G'$ at 250 Hz measured with a Rank Pulse Shearometer (solid symbols).

frequency behavior. Notice that there is no low-frequency plateau for any volume fraction, so from the dynamic experiments there is no indication of solidlike behavior.

### C. Influence of shear history, sample handling and storage on rheology

In Fig. 5 a compilation of $G'(\infty)$ and $G'$ (250 Hz) measured with different rheometers is shown as a function of volume fraction. For latex $A$ extrapolated values at 250 Hz from the low-frequency experiments are plotted since the Pulse Shearometer could not be used at these low

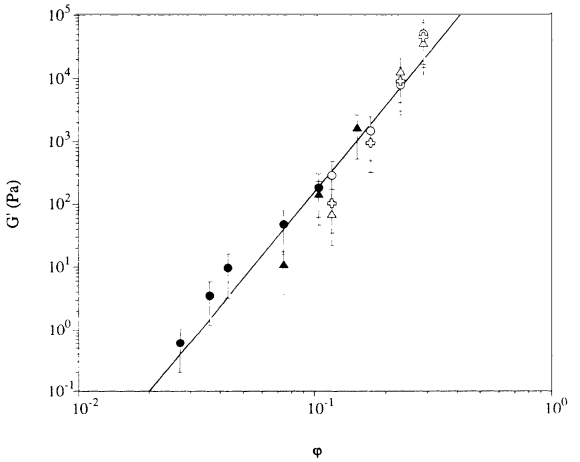


FIG. 5. Comparison of $G'$ obtained with different rheometers. Solid symbols, latex $A$; open symbols, latex $B$. The results were obtained with the controlled stress rheometer (○), a Bohlin VOR (△), and a Rank Pulse Shearometer (◇). The values obtained with the Bohlin are extrapolated to 250 Hz from low frequency data.

volume fractions. From Fig. 5, $G'$ does not seem to depend significantly upon the particle radius. When trying to compare the results of different rheometers, one encounters some problems which are inherent to the model system used. We investigated a number of possible sources of error:

*(1) Influence of waiting period.* It was found that the storage modulus increases on very long time scales. Only after 8.5 h did $G'$ no longer increase significantly. After the initial relatively fast increase of $G'$ due to formation of a space-filling network, a restructuring of the latter may occur on longer time scales, causing a slower increase of $G'$.

*(2) Short-term and long-term reproducibility.* The short-term reproducibility of the dynamic experiments, which was examined by refilling the rheometer and repeating the same experiment, is good. Over longer periods (several months), however, the reproducibility was worse. Hence, when comparing results of different rheometers, care should be taken to perform the experiments in as short a time period as possible after synthesis of the latex.

*(3) Influence of shear history and sample handling.* The exponent $\gamma_1$ derived in Sec. II C depends upon a number of structural parameters. Therefore, the amount of preshearing, which alters the microstructure of the sample, may be expected to influence the magnitude of $G'$. The hypothesis was verified by performing frequency sweeps after different shear histories (see Sec. III C 2). It was found that in some cases the moduli differed by a factor of about 2 depending on the shear rate applied during the preshearing period. Similar effects were also shown by recent computer simulations of Melrose and Heyes [28,29].

*(4) Extrapolation.* Due to the resolution of the time measurements (the angular displacements were measured at time intervals of 0.5 s), $J_g$ must be determined by extrapolation of the creep data. As a result, one in practice cannot extract $G'$ at *infinite* frequency from the creep experiments. Therefore, hereafter, if the quantity $G'(\infty)$ is used, we mean $G'$ at *high* frequencies relative to the characteristic frequencies of structural changes in the skeleton chains forming the space-filling network.

We conclude that considering differences in the experimental conditions between the various rheometers may add up to errors of roughly 70%. Applying a linear least-squares fit of (2.21) to all the data, one finds $\gamma_1 = 4.6 \pm 0.3$. The prefactor is about $6 \times 10^6$ Pa. The range of $\gamma_1$ found in this way overlaps the range $3.7 \leq \gamma_1 \leq 4.5$ found in the literature [7–9].

### D. Critical strain

In Fig. 6 the critical strain $\gamma_{\text{crit}}$ as a function of volume fraction is plotted. In the case of the Bohlin experiments, $\gamma_{\text{crit}}$ was determined from measurements at 1 Hz. For three volume fractions a number of shear stresses applied with the constant stress rheometer turned out to be high enough to cause nonlinear behavior. The $\gamma_{\text{crit}}$ in these cases were taken equal to the maximum strains at the onset of the nonlinearity. Since these estimations are rather crude, larger error bars are appropriate. Fitting the data to a power-law dependence [see Eq. (2.27)] yields $\gamma_3 = -2.5 \pm 0.3$. This result may be consistent with the values $\gamma_3 = -2.1$ and 2.3 found by Shih *et al.* [8]. In Sec. IV G we will come back to a discussion of $\gamma_3$ in relation to other structural parameters.

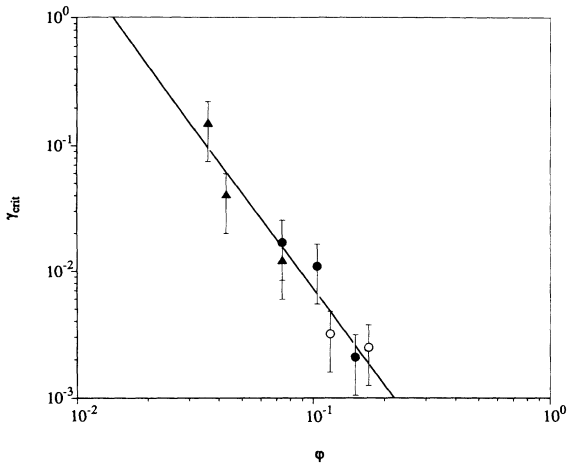


FIG. 6. Critical strain as a function of $\phi$. Solid symbols, latex *A*; open symbols, latex *B*. The results were obtained with the controlled stress rheometer (△) and a Bohlin VOR (○).

### E. Low-shear-limiting viscosity

Now we return to the question posed in the Introduction, i.e., whether or not the model system shows a yield stress. Since all creep experiments were done in the linear regime and the slope of $J(t)$ remains finite after imposing a stress, we must conclude that for none of the volume fractions considered was there a yield stress or a $G_0$ (see Sec. II A). From the slope of the master curve $M(t)$ just before cessation of the applied stress or its recovery after cessation of the stress, $\eta(0)$ can be found, as indicated in Fig. 1. The relative low-shear-limiting viscosity $\eta(0)/\eta_s$ ($\eta_s$ being the solvent viscosity) as a function of volume fraction for latex *A* and latex *B* is given in Fig. 7. The data can be fitted to a power law with a power $5.3 \pm 0.3$. The shear rates associated with the viscosities are as small as $10^{-8}$ s$^{-1}$ for the highest volume fraction.

In a recent paper Buscall, McGowan, and Morton-Jones [4] investigated wall slip in experiments on weakly aggregating dispersions. They pointed out that relative viscosities higher than $10^5$ will not occur unless the slip layer becomes undefinable, i.e., much smaller than one particle diameter. Since the viscosities we measured are of the order $10^5$ or higher, the conclusion that our experiments were not influenced by wall slip seems justified. As an illustration of the sensitivity of our instrument, we will give an example of the relative displacements in the creep experiments: From Fig. 1 one finds a low-shear-limiting viscosity of about $3 \times 10^4$ Pa. At a shear stress of 0.1 Pa and a gap width of 2 mm, particles at two sides of the gap are thus displaced at a rate of $7 \times 10^{-9}$ m/s relative to each other. After the 65 s during which the stress was

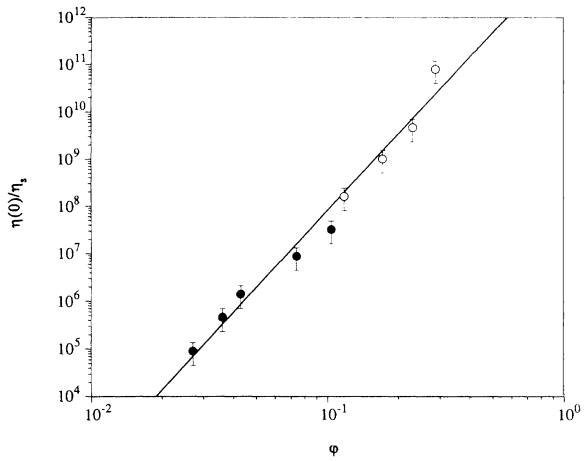


FIG. 7. Relative low-shear-limiting viscosity as a function of $\phi$. Viscosities were extracted from creep experiments. Solid symbols, latex $A$; open symbols, latex $B$.

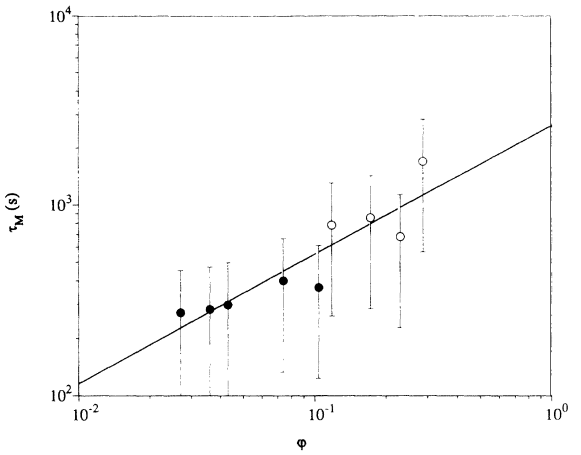


FIG. 8. Mean relaxation time as a function of $\phi$. Times were extracted from creep experiments. Solid symbols, latex $A$; open symbols, latex $B$.

applied, the maximum relative displacement of two particles is 450 nm, i.e., about one particle diameter. From this example one also may conclude that the occurrence of wall slip is unlikely.

### F. Comparison of characteristic time scales

An additional consistency check of the results may be provided by a comparison of the time scales extracted from the different experiments. Using (2.15), one easily obtains the mean relaxation times $\tau_M$ from the creep experiments. One of the primary quantities, i.e., $J_e$ as a function of $\phi$ is given in Table I [the viscosity $\eta(0)$ as a function of $\phi$ has already been given in Sec. IV E]. Also indicated in Table I is $\sum_k J_k = J_e - J_g$ as a function of $\phi$. Fitting of $J_e(\phi)$ to a power law gives a power $-4.7\pm0.3$.

In Fig. 8, $\tau_M$ as a function of $\phi$ is plotted for latex $A$ and latex $B$. Again, the data for latex $A$ and latex $B$ agree well. Fitting of the data to a power law yields a weak dependence upon $\phi$, i.e., $\tau_M \propto \phi^{0.7\pm0.6}$. The large error arises from a propagation of errors in $J_e$ and $\eta(0)$. Ladyzhinskii *et al.* [30] suggest

$$\tau_M = \tau_0 e^{U/k_B T}/N_{\rm ch}(\phi) \propto \phi^{d_{\rm ch}/(3-d_f)} .$$

In principle, $d_{\rm ch}$ can be determined with this expression if $d_f$ is known, but in this case the error in the exponent is so large that the value of $d_{\rm ch}$ obtained in this way would be of little interest.

The shortest time $\tau_M$ shown in Fig. 8 is $\tau_M \approx 260$ s at $\phi = 0.027$. The frequency

$$f_M = \frac{1}{2\pi\tau_M} \approx 6\times10^{-4} \text{ Hz}$$

associated with this value of $\tau_M$ is of the order of the lowest frequency $10^{-3}$ Hz applied in the dynamic measurements. Since the frequencies $f_M$ at all other $\tau_M$ are even smaller, a direct comparison is not possible. However, one sees from Figs. 3 and 4 that $\tau_M$ may indeed be larger than 260 s at $\phi > 0.027$, since all the curves of $G'$ are decreasing only slightly at frequencies around $10^{-3}$ Hz, indicating that a transition may occur at frequencies *lower* than $10^{-3}$ Hz. Hence, the dynamic and creep results are also not contradictory with respect to the characteristic time scales.

TABLE I. Steady-state compliance $J_e$ and $\sum_k J_k = J_e - J_g$ as a function of volume fraction. Data were obtained from controlled stress measurements on latex $A$ (upper five rows) and latex $B$ (lower four rows).

| $\phi$ | $J_e$ (1/Pa) | $\sum_k J_k$ (1/Pa) |
|---|---|---|
| 0.027 | $3.4\times10^{0}$ | $1.8\times10^{0}$ |
| 0.036 | $6.9\times10^{-1}$ | $4.0\times10^{-1}$ |
| 0.043 | $2.4\times10^{-1}$ | $1.4\times10^{-1}$ |
| 0.074 | $5.1\times10^{-2}$ | $3.0\times10^{-2}$ |
| 0.104 | $1.3\times10^{-2}$ | $7.5\times10^{-3}$ |
| 0.118 | $5.5\times10^{-3}$ | $2.1\times10^{-3}$ |
| 0.172 | $9.6\times10^{-4}$ | $2.9\times10^{-4}$ |
| 0.230 | $1.7\times10^{-4}$ | $4.1\times10^{-5}$ |
| 0.287 | $2.3\times10^{-5}$ | $3.1\times10^{-6}$ |

### G. Determination of structural parameters

In Sec. II C three expressions were given with which the three structural parameters $d_f$, $\varepsilon$, and $d_{\rm ch}$ can be determined from $\gamma_1$, $\gamma_2$, and $\gamma_3$. The exponents $\gamma_1$ and $\gamma_3$ have already been discussed in previous sections. It is at first sight tempting to use steady shear results to obtain $\gamma_2$, as was done in [3] by extrapolating the high-shear-rate behavior in a shear-rate versus shear-stress plot back to zero shear rate. In this way one determines the apparent Bingham stress or yield stress in shear. However, such a result in general cannot be combined with the exponents $\gamma_1$ and $\gamma_3$ extracted from *linear* measurements, since the former was obtained from a *nonlinear* experiment in which the structure is likely to be different from the equilibrium structure at rest. In other words, the structural parameters $\varepsilon$ and $d_{\rm ch}$ (and perhaps also $d_f$) may be different in both types of experiments. We will il-

lustrate this by using our previous data on the steady shear viscosity of the same model system [13] to determine $\gamma_2$ in steady shear. Following the same procedure as described in [3] to obtain the apparent Bingham stress as a function of volume fraction, we find $\gamma_2=2.0\pm0.1$. Using (2.24) and the bounds imposed on $\varepsilon$, we conclude that $0\leq\varepsilon\leq0.4$ for $1.8\leq d_f\leq2.0$. Values of $d_f>2.0$ give negative $\varepsilon$, while values of $d_f<1.8$ are excluded because they are unrealistically low.

Next we look more closely at the results obtained from the linear measurements. Using (2.21) and (2.27), one finds

$$2/(3-d_f)=\gamma_1+\gamma_3=2.1\pm0.4\ .$$

Hence, $d_f=2.0\pm0.2$, which overlaps with the range determined from the steady shear results. Thus, $d_f$ in rest does not seem to differ much from $d_f$ in shear. Since we have only two equations for three unknowns, we can only give lower and upper bounds of $\varepsilon$ and $d_{\rm ch}$. Again, using (2.21) and (2.27), one has

$$4\varepsilon+2d_{\rm ch}=(3-d_f)(\gamma_1-\gamma_3)=7.1\pm1.7\ .$$

Only certain combinations of $\varepsilon$ and $d_{\rm ch}$ are allowed within our model, because $0\leq\varepsilon\leq1$ and $1\leq d_{\rm ch}\leq\frac{5}{3}$. Hence, we find $0.5\leq\varepsilon\leq1$, while $1\leq d_{\rm ch}\leq\frac{5}{3}$. Clearly, the range obtained for $d_{\rm ch}$ is not informative, but comparing the range of $\varepsilon$ to the values $0\leq\varepsilon\leq0.4$ extracted from the steady shear experiments, one sees a difference, which may arise from a difference in structure. In the context of the model it is thus implied that in rest the skeleton chains are more or less isotropic, while in shear they are straighter. It corroborates the view that for aggregating systems one cannot combine results obtained by different types of experiments.

The presence of a difference in structure is further corroborated by the following: In Fig. 9 we plotted the viscosities at low and high shear rates against shear stress. The former were obtained with creep experiments on latex $A$ ($\phi=0.043$, radius 200 nm), while the latter were measured with a Contraves low shear rheometer [13] on a different latex batch ($\phi=0.045$, radius 220 nm). Notice that the creep experiments were indeed done in the linear regime. It is evident from Fig. 9 that the experiments starting from a high shear rate do not connect smoothly with the experiments starting from the rest structure. This too is an indication of a different structure in both cases, which also confirms the point we made in Sec. IV C on the influence of shear history on rheological properties.

The range found for $d_f$ is consistent with the value $d_f=2.03$ obtained from computer simulations including random breakup of bonds [6]. Our data also are consistent with the data given in [11], which were obtained from computer simulations on fractal trees. For a fractal dimension $d_f=2.05\pm0.15$, it was found that $\varepsilon=0.87\pm0.20$ and $d_{\rm ch}=1.7\pm0.1$, resulting in $4\varepsilon+2d_{\rm ch}=6.9\pm1.0$. The latter value agrees well with the value $7.1\pm1.7$ obtained from the linear experiments. The computer simulations in [11] were done for rigid structures but did not include thermal breakup of bonds. In summary, we conclude that the data can be interpreted quantitatively using equations based on *bond-bending* interactions. We think this is the first time that an attempt has been made to relate the three exponents $\gamma_1$, $\gamma_2$, and $\gamma_3$ to the three relevant structural parameters $d_f$, $\varepsilon$, and $d_{\rm ch}$.

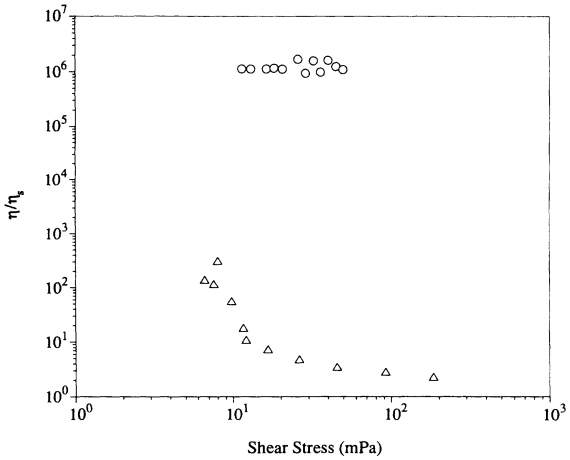


FIG. 9. Relative viscosity as a function of shear stress, illustrating the influence of the microstructure on rheological properties. Viscosities were extracted from creep measurements (○) and steady shear measurements (△). The latter were performed with a Contraves low shear rheometer and described in [13].

## V. DISCUSSION AND CONCLUSIONS

Using a sensitive controlled stress rheometer developed in our laboratory, we have studied the creep behavior of two weakly aggregating polystyrene latex dispersions in the linear regime. The high-frequency storage moduli $G'(\infty)$ extracted from the creep experiments are consistent with moduli obtained with dynamic measurements.

Additional information obtained from the creep measurements are the steady-state compliance and the steady shear viscosity at low shear rates, from which we deduced a mean relaxation time $\tau_M$. Measurements of the creep behavior at a number of volume fractions between 0.02 and 0.30 all show the *absence* of a yield stress or equilibrium modulus. The low-shear-limiting viscosity or Newtonian plateau is as high as $7\times10^7$ Pa s at the highest volume fraction, while the lowest shear rates associated with this viscosity are of the order of $10^{-8}$ $s^{-1}$. The mechanism responsible for the Newtonian plateau is thermal breakup of bonds. The absence of an equilibrium modulus is corroborated by the dynamic experiments, which do not show a low-frequency plateau.

The high-frequency modulus as a function of $\phi$ shows a power-law dependence with a power $\gamma_1=4.6\pm0.3$. The magnitude of the modulus appears to depend strongly on the shear history (i.e., structure) of the sample. Also, $G'$ increases on very long time scales ($\approx8.5$ h). Hence, caution should be taken to apply similar shear histories when results of different apparatus are to be compared.

Using an additional exponent, i.e., $\gamma_3=-2.5\pm0.3$, describing the scaling of the critical strain below which

the material behaves linearly, the fractal dimension $d_f$ and the lower and upper bounds of the structural parameter $\varepsilon$ were determined with a model based on bond-bending interactions.

When dealing with the *dynamic* moduli described in Sec. III, there is an additional possibility (besides those mentioned in the Introduction) which in principle could explain apparent bond-bending behavior. In the Kantor and Webman approach the elasticity is described in terms of loaded skeleton chains forming the network. Branches and dangling (i.e., unloaded) bonds are neglected. However, due to a branch, two particles near it are not able to move affinely since they sense the presence of a third particle. The latter introduces an *effective* bond-bending component in the two-particle interaction potential at high frequencies, because the time scales involved may be too short for the force of a third particle to relax. In our description in Sec. II C, dangling bonds or branches have been neglected but actually there may be quite a large amount of them [6]. Hence it seems not unreasonable to consider a model based on unbranched chains where the "error" made in neglecting the branches is felt as an apparent bond-bending component in the interparticle potentials. This assumption has been corroborated by the reasonable agreement with the simulation results [11].

This fact we consider an intermediate research stage. Though often used, the static picture of a number of elastic chains as outlined in Sec. II C is clearly not very sophisticated. The microstructural picture of the model system is one in which there are *temporary* bonds between aggregates, because of the absence of a rest shear modulus. The kinetics of creation and breakup of these bonds should in fact be taken into account. Thus the static model does not account for the volume-fraction dependence of the stationary number of bonds. The latter would also result in a volume-fraction-dependent prefactor of $G'(\infty)$, which would be different from the prefactor of $G_0$.

Moreover, the question of the irrelevance of central forces has not yet been settled. Indeed, it is not easy to see how fractal structures with relatively low fractal dimensions $d_f$ can be formed from particles having only central interactions, since in that case finite volume effects are the only factor preventing compact structures. It was shown by computer simulations [6] that in the case of diffusion-limited cluster-cluster aggregation, the fractal dimension of the aggregates is increased from 1.89 in the absence of reinstructing to 2.08 in the presence of restructuring due to rotations of the two parts of the aggregate after they made contact. Other aggregation mechanisms give somewhat higher fractal dimensions. However, experimentally found values of $d_f$ cannot be used to determine whether or not the interactions are central, because $d_f$ is also affected by thermal breakup of bonds. It was found that in the case of diffusion-limited cluster-cluster aggregation with random bond breaking, $d_f$ increased from 1.89 to 2.03 [6]. Since for our model system one may expect thermal breakup to occur, an experimentally determined value of $d_f \approx 2$ does not necessarily mean that we are dealing with central interactions only. Hence, we have no experimental evidence in favor of or against noncentral interactions. It would therefore be interesting to develop a model based on central interactions and to reconsider the results in terms thereof.

## ACKNOWLEDGMENTS

The authors wish to acknowledge C.A.J. Damen for carrying out the dynamic experiments on latex *B* and J. S. Lopulissa for his work on the synthesis of the polystyrene model latices. The work described in this paper is part of the research program of the Stichting voor Fundamenteel Onderzoek der Materie (FOM), which is financially supported by the Nederlandse Organisatie voor Wetenschappelijk Onderzoek (NWO).

[1] R. C. Sonntag and W. B. Russel, J. Colloid Interface Sci. **116**, 485 (1987).
[2] M. Chen, and W. B. Russel, J. Colloid Interface Sci. **141**, 564 (1991).
[3] R. Buscall, I. J. McGowan, and C. A. Mumme-Young, Faraday Disc. Chem. Soc. **90**, 115 (1990).
[4] R. Buscall, I. J. McGowan, and A. J. Morton-Jones, J. Rheol. **37**, 621 (1993).
[5] D. P. Patel and W. B. Russel, Colloids Surf. **31**, 355 (1988).
[6] P. Meakin, Adv. Coll. Polym. Sci. **28**, 249 (1988).
[7] R. Buscall, P. D. A. Mills, J. W. Goodwin, and D. W. Lawson, J. Chem. Soc. Faraday Trans. 1 **84**, 4249 (1988).
[8] W. Shih, W. Y. Shih, S. Kim, J. Liu, and I. A. Aksay, Phys. Rev. A **42**, 4772 (1990).
[9] R. Vreeker, L. L. Hoekstra, D. C. Den Boer, and W. G. M. Agterof, Colloids Surf. **65**, 185 (1992).
[10] W. D. Brown, Ph.D. thesis, Cambridge University, 1986).
[11] A. A. Potanin, J. Colloid Interface Sci. **157**, 399 (1983).
[12] S. Feng and P. H. Sen, Phys. Rev. Lett. **52**, 216 (1984).
[13] R. De Rooij, A. A. Potanin, D. Van den Ende, and J. Mellema, J. Chem. Phys. **99**, 9213 (1993).
[14] T. A. Witten, L. Leibler, and P. A. Pincus, Macromolecules **23**, 824 (1990).
[15] Y. Rabin and S. Alexander, Europhys. Lett. **13**, 49 (1990).
[16] J.-L. Barrat, Macromolecules **25**, 832 (1992).
[17] J. Klein, Pure Appl. Chem. **64**, 1577 (1992).
[18] J.-F. Joanny, Langmuir **8**, 989 (1992).
[19] J. W. Goodwin, R. W. Hughes, S. J. Partridge, and C. F. Zukoski, J. Chem. Phys. **85**, 559 (1986).
[20] D. Van den Ende, R. De Rooij, C. Blom, E. G. Altena, G. J. Beukema, and J. Mellema (unpublished).
[21] N. W. Tschoegl, *The Phenomenological Theory of Linear Viscoelastic Behavior* (Springer-Verlag, Berlin, 1990).
[22] A. A. Potanin, J. Colloid Interface Sci. **145**, 140 (1991).
[23] Y. Kantor and I. Webman, Phys. Rev. Lett. **52**, 1891 (1984).
[24] P.-G. De Gennes, *Scaling Concepts in Polymer Physics* (Cornell University, Ithaca, 1979).

[25] H. J. Hermann and H. E. Stanley, Phys. Rev. Lett. **53**, 1121 (1984).
[26] R. Wessel and R. C. Ball, Phys. Rev. A **46**, R3008 (1992).
[27] J. W. Goodwin, J. Hearn, C. C. Ho, and R. H. Ottewill, Coll. Polym. Sci. **252**, 464 (1974).
[28] J. R. Melrose and D. M. Heyes, J. Colloid Interface Sci. **157**, 227 (1993).
[29] J. R. Melrose and D. M. Heyes, J. Chem. Phys. **98**, 5873 (1993).
[30] I. Y. Ladyzhinskii, G. N. Ureva, J. Mewis, and N. B. Urev, Kolloidn. Zh. **54**, 97 (1991) [Colloid J. USSR **54**, 77 (1992)].